

# Evidence for the formation of CCN by photochemical processes in Mexico City

D. Baumgardner\*, G.B. Raga, A. Muhlia

*Universidad Nacional Autónoma de México Mexico City, Mexico*

Received 15 May 2003; accepted 3 October 2003

## Abstract

Cloud condensation nuclei (CCN) concentrations in Mexico City have a diurnal cycle that is similar to those of condensation nuclei (CN) and  $PM_{2.5}$  but CCN, on average, lags the changes in CN and  $PM_{2.5}$  by almost an hour. The nature of these patterns is related to the onset of emissions from vehicular traffic in the morning followed by the photochemical production of secondary organics that condense on the primary particles. The rates at which particles grow and the detection thresholds of the instruments that measure them impose the apparent lag in CCN trends. A size-resolved aerosol model simulates the observed trend when instrument thresholds and boundary layer growth are taken into account. The measurements made in the year 2000 show no discernible decrease in maximum daily CCN concentrations when compared to similar measurements made in 1984, despite the efforts of local authorities to decrease pollution levels in Mexico City.

© 2003 Elsevier Ltd. All rights reserved.

*Keywords:* CCN; Secondary organics; Mexico City

## 1. Background

Observational studies have shown that anthropogenic cloud condensation nuclei (CCN), e.g., those formed from biomass burning or urban emissions, can impact the local or regional development of clouds and precipitation (e.g., Fitzgerald and Spyers-Duran, 1973; Hindman et al., 1977; Changnon et al., 1981; Rosenfeld, 2000). All the studies showed evidence that the average cloud droplet size was smaller and total concentration much higher in clouds that are influenced by anthropogenic CCN than those that are not. The change in cloud microstructure has two consequences: (1) clouds with higher droplet concentrations are more reflective of solar radiation and (2) precipitation develops more slowly, or not at all, if droplets remain too small to coalesce or grow by condensation to raindrop sizes. The first consequence impacts climate while the second

impacts the water cycle; hence the need to understand processes that affect the production and evolution of CCN.

There is a paucity of CCN measurements in heavily populated and industrialized areas. Most CCN measurements have been made in cities with populations less than a million (e.g., Alofs and Liu, 1981; Hudson and Frisbie, 1991; Hitzenberger et al., 1999). Only a few from larger population centers have been published, e.g. from Washington, DC (Fitzgerald et al., 1982) and Mexico City (Herrera and Castro, 1988; Montañez and García-García, 1993). The Mexico City measurements reported in this study augment the current data base of measurements from very large urban areas and suggest that the production of CCN, as well as CN and  $PM_{2.5}$ , is strongly linked to secondary, photochemical processes.

## 2. Measurement program

Measurements were made 13–29 September, 2000 on the campus of the Universidad Nacional Autónoma de

\*Corresponding author. Fax: +52-555-622-4248.  
E-mail address: darrel@servidor.unam.mx  
(D. Baumgardner).

México (UNAM) that is located in the southwest sector of the Mexico City basin. The instrumentation consisted of sensors for meteorological conditions, solar radiation and particle number and CCN concentration. The global and UV-A component of the solar radiation were measured with Eppley<sup>1</sup> hemispheric radiometers and the diffuse component with a Kipp and Zonen<sup>2</sup> radiometer. Total aerosol number concentration measurements, for diameters larger than 0.01  $\mu\text{m}$ , were made with a TSI<sup>3</sup> model 3010 CN counter. The concentrations were corrected for coincidence losses (multiple particles counted as one) using the algorithm provided by the company.

Measurements of CCN were made with a University of Wyoming counter (Delene et al., 1998). This instrument is a parallel plate, static, thermal-gradient diffusion cloud chamber (SDCC) that takes an air sample and makes a measurement approximately every 60 s. Particles with critical supersaturations less than the controlled value activate and grow in the instrument chamber to the size of cloud droplets within about 20 s. A laser illuminates these droplets and the scattered light intensity is collected and focused on a photodetector. The output of this detector is recorded and converted to a particle number concentration based on calibrations.

The relationship between droplet concentration and scattered light is determined using monodispersed aerosols produced with an ultrasonic nebulizer and size-selected with an electrostatic classifier. The sample volume is viewed with a high-resolution digital camera and the activated particles are counted for different values of the supersaturation and particle concentration. The accuracy of this calibration procedure, a function of the supersaturation, is  $\pm 10\%$  (Delene and Deschler, 2000). Nenes et al., (2001) simulated a number of different types of CCN counters and concluded that the SDCC, for a fixed supersaturation, produces monodispersed droplets with less than 10% variation. Uncertainties associated with wall temperature boundary conditions were found to be negligible.

The accuracy of CCN counters is limited by uncertainties due to supersaturation, sensitivity to fluctuations in the temperature control and vapor gradients in the chamber, accuracy of calibrating the concentration versus light scattering and changes in particle composition prior to measurement, to name just a few. (Chuang et al., 2000). The primary intent of the present study is to report on the importance of secondary, photochemical processes in the production of CCN. As such, the focus is on the relative, diurnal changes rather than the absolute magnitudes.

The government of Mexico City operates a network of 36 environmental monitoring stations, the Red Automática de Monitoreo Atmosférico (RAMA). One of these stations, 4 km from the UNAM site, measures carbon monoxide (CO), ozone (O<sub>3</sub>), nitrogen oxides (NO<sub>x</sub>), sulfur dioxide (SO<sub>2</sub>) and the mass concentration of particles with aerodynamic diameters less than 2.5  $\mu\text{m}$  (PM<sub>2.5</sub>). The PM<sub>2.5</sub> is measured with a tapered element oscillating microbalance (TEOM) manufactured by Rupprecht and Patashnick.<sup>4</sup> The TEOM was operated at 50°C to remove water from the particles. As discussed below, semi-volatile organics may also be removed at this temperature (Allen et al., 1997). The RAMA data were provided as hourly averages, the meteorological and radiation data were 10 min averages and the CN measurements were recorded at 1 Hz and averaged to 1 min intervals. The CCN cloud chamber pads required moistening approximately every 2–3 h. This limited the daily operation of the counter from 6 AM to 10 PM.

The supersaturation of the CCN counter was cycled from 0.2% to 0.6% in 0.1% steps. A reading at each supersaturation takes approximately 1 min, thus requiring 5 min for a complete sequence. The concentration of CCN at supersaturations larger than 0.6% exceeded the maximum range of the counter. The expected uncertainty in the measurements, based upon the analysis of others (Chuang et al., 2000; Delene and Deschler, 2000) is on the order of 20% at all supersaturation settings.

### 3. Results

September is normally a month of frequent rain in Mexico City. The cloud cover varied from scattered to overcast throughout the research period, with one extended segment, the 14th–18th, when daily afternoon rain showers occurred. Fig. 1 illustrates the general trends in winds, relative humidity (RH) and ultra-violet (UV-A) radiation during the 2-week period. The displayed values are 6 h averages. The sampling period is separated into two general categories: (1) partly cloudy with no rain and (2) cloudy with occasional precipitation. On days in the first category (13 September and 19–23 September) the winds were from the east-southeast and maximum UV-A levels varied from 20 to 40  $\text{W m}^{-2}$ . The RH decreased from nighttime highs of 90% to values less than 60% during the day. During the second category days (14–18 September), daytime winds were from the northwest, the RH remained high between 75% and 100%, and the maximum UV-A radiation was about half of cloudless values. The period from 24–28 September had no rain, but the winds, UV-A and RH were similar to the rainy period. The analysis presented here is only from days in the first category.

<sup>1</sup> Eppley Laboratories, Newport, RI.

<sup>2</sup> Bohemia, NY.

<sup>3</sup> Thermo-Systems Incorporated, Shoreview, MN.

<sup>4</sup> Rupprecht & Patashnick Co., Inc., Albany, NY.

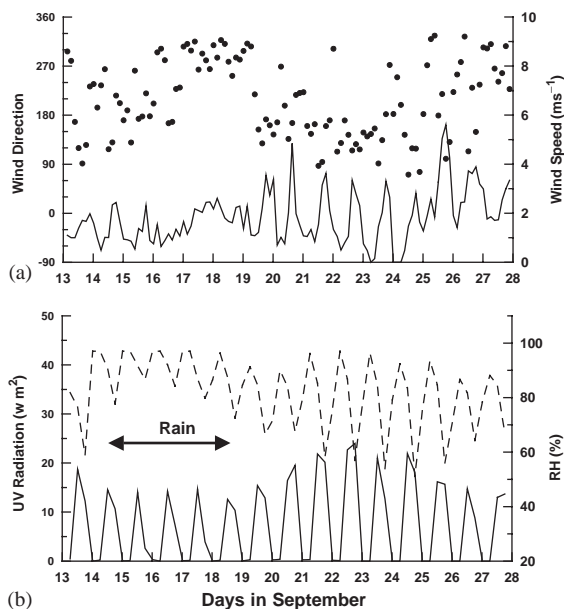


Fig. 1. Time series of meteorological data during the measurement program are shown. Panel (a) is the wind direction (circles) and speed (solid line). Panel (b) shows the UV radiation (solid line), relative humidity (dashed line) and rainy period (line with arrows).

The daily trends in CN, CCN and  $PM_{2.5}$  were generally the same each day. The six panels of Fig. 2 are time series of these parameters, averaged over 20 min intervals. The time series of 13th September is representative of a daily pattern. The concentrations of all three parameters are moderately low prior to 0600 local standard time (LST), after which CN increases steadily for 2 h and peaks between 0800 and 0900. The  $PM_{2.5}$  begins increasing at approximately the same time as the CN and, with the exception of the 21st and 22nd, the  $PM_{2.5}$  reaches a plateau simultaneous with the CN. Unlike the CN, however, the  $PM_{2.5}$  begins to increase again and reaches a higher peak several hours later. This second maximum is generally found within an hour of the first peak in CCN.

The CCN begins to increase 1 to 2 h after the rise in CN and reaches the first maximum around 1100 or 1200, or about 3 to 4 h after the peak in CN. The CCN generally decreases throughout the afternoon but reaches a second, smaller maximum between 1800 and 2200. This peak corresponds in time to a similar peak in CN and  $PM_{2.5}$ .

Fig. 3 shows the daily variations in UV-A radiation and RH. Daylight arrives prior to 0600 but the eastern mountain range obstructs direct sun until after 0600 when there is a rapid increase in radiation, reaching a maximum around 1300. The fluctuations attest to the cloudiness during the day; however, the radiation

exceeds  $30 \text{ W m}^{-2}$  prior to the onset of clouds on all days. In September the sun moves below the western mountain range at 1700 but daylight persists until after 1800. The RH is high at night but decreases throughout the day until sunset.

Traffic throughout the city begins to increase at 0600 as reflected in the CO trends measured at the RAMA station and shown in Fig. 4. The exception to this is on 23 September, a Saturday, when CO does not begin increasing until 0800. There is a six-lane road 300 m to the east of the research site that is used by a variety of vehicles. The subway station and a bus terminal are also located in this area. The emissions from vehicles in this area, as well as the university traffic on nearby streets, are a strong source of fresh particle and gas emissions.

There was no CO measurement at the UNAM research site, but a comparison of CO measurements from several of the RAMA stations in the southern part of Mexico City indicates that CO trends are almost identical, i.e. CO increases and peaks at approximately the same hour at four locations within a radius of 5 km from UNAM. Hence, we assume that CO measured at the nearby RAMA station represents trends in CO at the UNAM site. The CO starts to increase at the same time as CN; however, the rate is slower and reaches a maximum 1 to 2 h after the first peak in CN. Also shown in this figure is the  $O_3$  whose concentration is linked to the photochemical reactions involving  $NO_x$  and volatile organic compounds (VOCs).

The trends in CO and particles are not correlated with wind direction or velocity. The wind is generally calm until early afternoon before increasing to a maximum in the late afternoon.

Results from the April, 1984 study in Mexico City (Herrera and Castro, 1988) report average maximum CCN values of  $\approx 6000 \text{ cm}^{-3}$  at 1% supersaturation. Average maxima measured the following year in August, 1985 were of the same magnitude (Montañez and Garcia-Garcia, 1993). In addition, this latter study made CN measurements with an Aitken counter that ranged from 20,000 to 200,000  $\text{cm}^{-3}$ . The maximum CCN in the present study ranged from 2000 to 3000 at 0.5% supersaturation and the CN from 30,000 to 60,000  $\text{cm}^{-3}$ . Note that the Aitken counter in the 1985 study had a lower size threshold of 0.003  $\mu\text{m}$ , whereas the counter in the current study can measure to 0.01  $\mu\text{m}$  (Quant et al., 1992). This excludes a significant fraction of the small particles that are seen by the more sensitive counter. The maximum CCN concentrations reported in the current study, that are of similar magnitude to the measurements made 15 years previously, suggests that pollution mitigation efforts by the local authorities, focused on reducing ozone, have had little effect on hygroscopic particle concentrations.

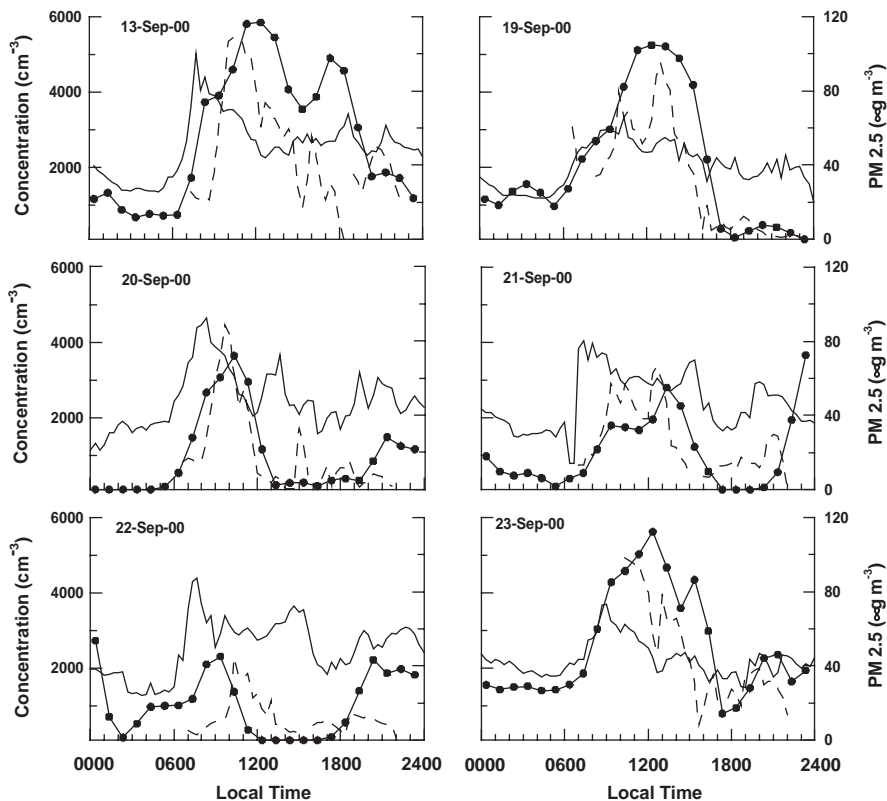


Fig. 2. Time series of  $CN \div 10$  (solid),  $CCN$  (dashed) concentrations, at 1% supersaturation, in  $cm^{-3}$  and  $PM_{2.5}$  mass (circles) in  $\mu g m^{-3}$  for the six case studies.

#### 4. Discussion

The trends in  $CO$ ,  $CN$ ,  $CCN$  and  $PM_{2.5}$  reflect a diurnal pattern that is correlated with primary emissions of motor vehicles. The differences in when the maxima occur for the gases and particles and the rates at which they increase imply that several physical processes are affecting the production of these species.  $CO$  is a sensitive tracer for primary emissions since combustion is the main source of this gas in urban environments.  $CO$  also has a long lifetime since the primary sink, oxidation by  $OH$ , is a slow removal mechanism (Seinfeld and Pandis, 1996). Hence, the  $CO$  trends reflect not only emissions but also dilution by mixing with free tropospheric air as the boundary layer increases during the day (Raga et al., 1999).

The differences in trend between  $CN$  and  $CO$  suggests other primary or secondary sources in addition to combustion. Likewise, since the trends in  $CCN$  and  $PM_{2.5}$  do not match those of  $CO$  or  $CN$ , other processes are likely involved in their formation as well.

The diurnal change in particle concentration and mass has been noted in previous studies. The 1984 Mexico City study (Herrera and Castro, 1988) reported daily

cycles with  $CCN$  maxima that occur between 0730 and 1000 LST. The 1985 Mexico City study (Montañez and Garcia-Garcia, 1993) examined the  $CCN$  and  $CN$  patterns in greater detail, accompanied by measurements of  $NO$ ,  $NO_2$  and  $SO_2$ . The experimenters noted that the peak in  $NO$  and  $NO_2$ , products of combustion like  $CO$ , preceded that of  $CCN$ ; however, they do not compare trends in  $CN$  with  $CCN$  or the gases. The authors concluded that trends in  $CCN$  were related to traffic activity, that photochemical reactions might play a role in the  $CCN$  formation, but that the processes were complicated and merited further measurements and analysis.

A study in an urban area of the United Kingdom (Harrison et al., 1999) reported diurnal variations in  $CN$ ,  $PM_{10}$  and surface area. No  $CCN$  measurements were made but the importance with respect to the current study is that the authors observed that morning increases in  $PM_{10}$  and surface area did not start until almost an hour after the rise in  $CN$ . They were unable to show correlations with wind speed but hypothesized that photochemical processes were forming hygroscopic material on particles that subsequently grew by deliquescence.

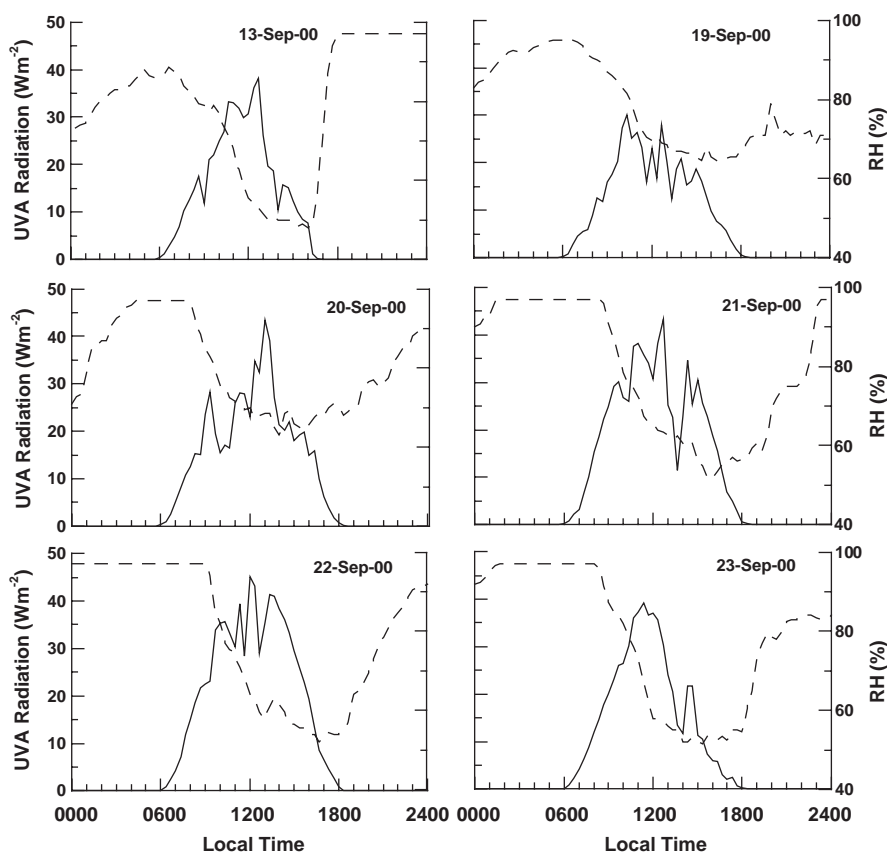


Fig. 3. Time series of global radiation (solid) and relative humidity (RH, dashed) for the six case studies.

Four independent studies, including the present one, show similar results with respect to the difference in CN trends compared to other pollutant species in urban areas. The trends and the phase differences of significant features are not correlated with wind speed in the these studies, but photochemical processes, as suggested in two of the three previous studies, is a factor that is explored further here.

The oxidation and hydration of soot as a source of hygroscopic particles has been proposed by a number of investigators. Laboratory studies have been conducted in which soot is exposed to extremely high concentrations of ozone (e.g., Chughtai et al., 1999; Smith and Chughtai, 1997), after which the soot was found to be hygroscopic. This process might explain the delay between the CCN formation and CN since soot is formed during combustion and ozone is produced by photochemical reactions. The ozone used in those studies, however, was several orders of magnitude higher than found in urban environments. Other studies using more realistic levels of ozone (Kotzick et al., 1997; Kotzick and Niessner, 1999) also found increases in hygroscopicity after soot was treated with ozone. Five hours of aging were needed to change pure carbon

aerosols from hydrophobic to hydrophilic within the atmospheric CCN supersaturation range. These studies have limited relevance since soot in ambient air will absorb a variety of gases and can act as a catalyst for oxidation of species that lead to the formation of hygroscopic material.

Some organic carbon compounds are hygroscopic, particularly organic acids (Yu, 1999 and references therein). These acids form by gas-to-particle conversion or condensation of low volatility gases, many of which are products of photochemical reactions with organic compounds emitted during combustion (Jenkin and Clemenshaw, 2000 and references therein).

The generation of secondary organic aerosols (SOA) from photochemical processes can help explain the observed trends in CN with respect to CO and CCN, if a fraction of the CN, as well as CCN, are SOA. The smallest particle size that can be measured with 100% efficiency by the CN counter used in the present study is approximately  $0.05 \mu\text{m}$ , with 50% efficiency at  $0.03 \mu\text{m}$  (Quant et al., 1992). High concentrations of soot particles are initially emitted by combustion with initial sizes much smaller than  $0.01 \mu\text{m}$  but coagulate rapidly to average diameters between  $0.04$  and  $0.10 \mu\text{m}$  (Harris and

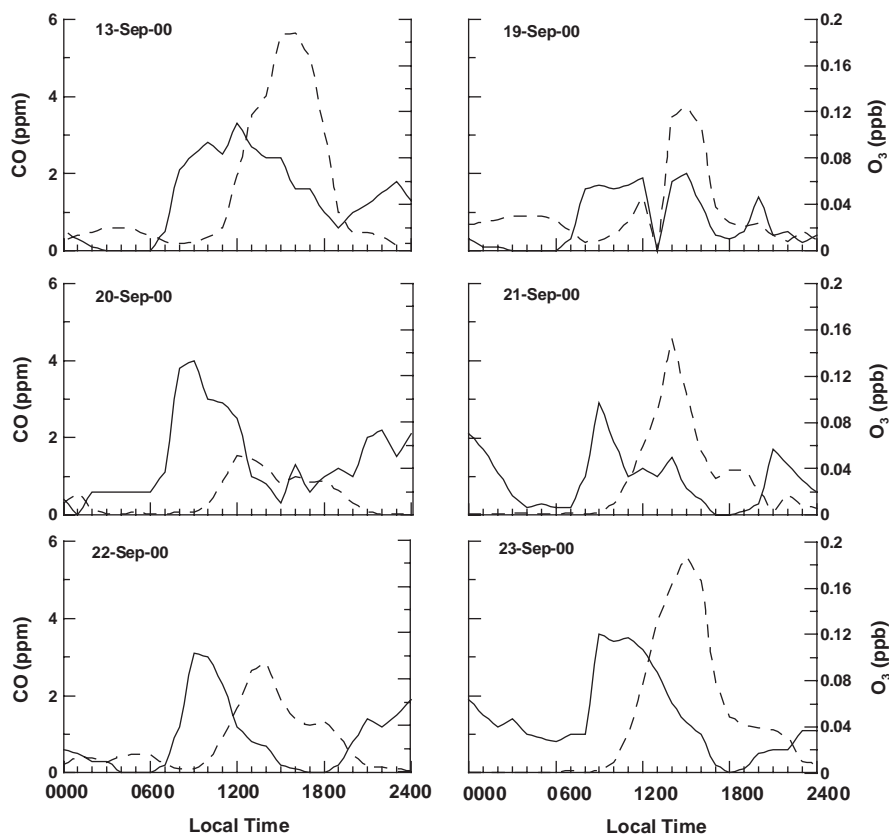


Fig. 4. Time series of carbon monoxide (CO, solid) and ozone ( $O_3$ , dashed) for the six case studies.

Maricq, 2001). Hence, the CN counter is detecting only a small fraction of the initially emitted particles. These particles continue to grow when low vapor pressure inorganic and organic gases condense on their surfaces. Some of these low vapor pressure species are gases formed by combustion but other studies have shown (Odum et al., 1996, 1997; Jenkin and Clemitshaw, 2000) that aromatics, alkanes and olefins, formed from photochemical reactions, produce the highest yield of SOA.

The same argument explains the production of CCN by secondary photochemical processes. Corrigan and Novakov (1999) show that the activation diameter of an organic aerosol, as a function of supersaturation, is related to its composition using Köhler theory, e.g., at a supersaturation of 0.5%, succinic and adipic acids activate when they have diameters of 0.064 and 0.12  $\mu\text{m}$ , respectively. If these, and other carboxylic acids known to be CCN, grow by condensation of secondary gases on primary particles, then they will grow until they reach a diameter at which they will activate as CCN for a given supersaturation.

An aerosol box model is used to test the hypothesis: the trends in CN and CCN concentrations are a result of

particles that are produced by primary emission and grow by condensation until they reach a detectable size. The corollary is: the principal gases that condense onto particles are produced by photochemical processes.

The model is an adaptation of a size-resolved, multicomponent model of urban and regional aerosol (Wexler et al., 1994; Sun and Wexler, 1998; Durlak et al., 1999) and uses meteorological and geographical conditions for Mexico City. The gas phase photochemical module is based on the model developed by Carter (1990). The organics are lumped into generic classes and the secondary organic aerosol production is estimated based on aerosol yields from smog chamber experiments and estimations based on reactivity and volatility of the products (Odum et al., 1996, 1997). All low vapor pressure, secondary organics that are produced are assumed to condense onto the aerosol. Coagulation is not incorporated into the model since coagulation is only a factor when particle concentrations are greater than  $10^6 \text{ cm}^{-3}$  (Zhang and Wexler, 2002). This model assumes that the coagulation occurs immediately after combustion when this process quickly moves the majority of the particle mass to sizes larger than 0.01  $\mu\text{m}$  (Harris and Maricq, 2001). The size distribution

is divided into 64 channels whose widths increase logarithmically from 0.01 to 18  $\mu\text{m}$ .

The model assumes that the aerosols are an external mixture of sulfate, elemental carbon and crustal material in addition to the organic material. The focus of the present work is to study changes of the organic component, hence only the organic size distributions are discussed in this analysis. Clearly sulfate particles will contribute to the particle population but their formation and growth are only loosely linked to the photochemical processes that are being examined here.

The model assumes a constant emission of gases and particles between 0600 and 1800 and solar zenith angles that change based on the location of Mexico City, the time of the year and hour of day for the project. The gases used in this application of the model are CO, NO, NO<sub>2</sub> and hydrocarbons, whose composition and concentrations are based on the most recent inventory and source apportionment for Mexico City (Vega et al., 2000). The CO, NO, and NO<sub>2</sub> values are averages of the RAMA measurements made at 0600 over the two week period of the project. The input size distribution is log

normal with average diameter and variance reported from measurements of fresh diesel and gasoline engine emissions (Harris and Maricq, 2001). The composition is organic with no speciation by functional group. The total number concentration is based on the average maximum value measured on the 6 days used in the present study.

The number size distributions are integrated from 0.03 to 18  $\mu\text{m}$  to obtain a total number concentration that simulates the measurement by the CN counter. The CCN measurements are simulated by integrating the size distributions calculated during the second run from 0.06 and 0.1  $\mu\text{m}$  to 18  $\mu\text{m}$ . The two thresholds were selected based on studies that show that the common organic acids (succinic and adipic) have activation diameters at 0.5% supersaturation that are on the order of 0.06 and 0.1  $\mu\text{m}$ , respectively (Cruz and Pandis, 1997; Corrigan and Novakov, 1999; Hori et al., 2003). The mass size concentrations were integrated from 0.05 to 2.5  $\mu\text{m}$  to simulate measurements of PM<sub>2.5</sub>. Fig. 5 shows the number (bottom panel) and mass (top panel) size distributions at 6, 8 and 10 h local time (solid, dashed

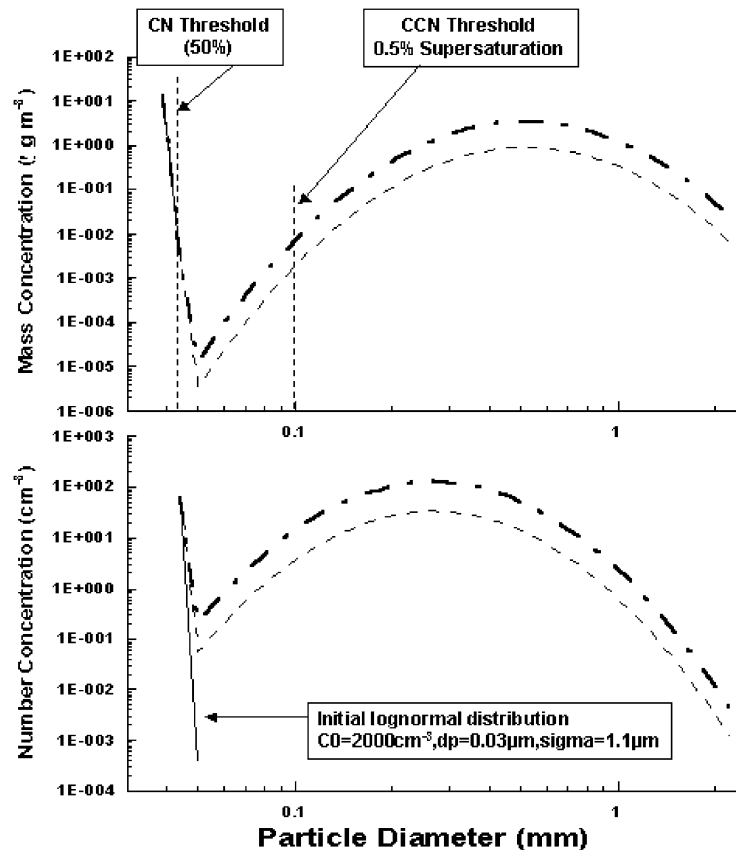


Fig. 5. The simulated size distributions of mass (upper panel) and number (lower panel) concentrations are shown at 0600 LST (solid), 0800 (dashed) and 1000 (dot-dash). The dashed lines at 0.03 and 0.1  $\mu\text{m}$  are the simulated, lower size thresholds for the 3010 CN counter and CCN counter at 0.5% supersaturation, respectively.

and dot-dash lines, respectively). Also indicated in the figures are the lower size thresholds assumed for the CN and CCN measurements. The size segment from 0.05 to 1  $\mu\text{m}$  is selected in the figures in order to highlight how the particles grow into the size ranges of the instruments.

Fig. 6, top panel, summarizes the results of the simulated concentrations of CN (solid line) and the CCN at 0.06  $\mu\text{m}$  critical diameter (dashed) and 0.1  $\mu\text{m}$  (dot-dashed). In the bottom panel is the simulated  $\text{PM}_{2.5}$  mass. The emissions are started at 0600 but the concentrations and mass show no significant increase until after 0630, the time of sun rise. The CN and  $\text{PM}_{2.5}$  have the same trends and the CCN increases at a slower rate than the CN and  $\text{PM}_{2.5}$ . The CCN concentration simulated at a 0.1  $\mu\text{m}$  diameter critical radius shows a slower increase with time than the 0.06  $\mu\text{m}$  threshold diameter. The model produces the general, morning features seen in the observations; however, as the model proceeds, the concentration of all three types of particle continues to increase. This is not seen in the observa-

tions, except for the modest increase in the afternoon that is probably due to lunch hour traffic. In general, the observed concentrations decrease after reaching their highest peaks in the late morning.

The aerosol model does not account for increases in the height of the mixing layer that dilutes the concentration of particles and gases during the day, reflected in the CO observations (Raga et al., 1999). There are fluctuations in the vehicular emission rates during the day; however, starting at 0600 and lasting until the end of the evening rush hour, the emissions normally remain high and the decrease that is seen in CO after 0900 (Fig. 4) is primarily the result of dilution by turbulent mixing with free tropospheric air. A second-order polynomial was fit to the average CO values between the average maximum at 1000 and minimum at 1800 for the 6 days of the analysis and then normalized to unity by the maximum value. The number and mass concentrations were then multiplied at each time step after 0900 by this function to include the effect of dilution. Fig. 7 shows the results of this modification

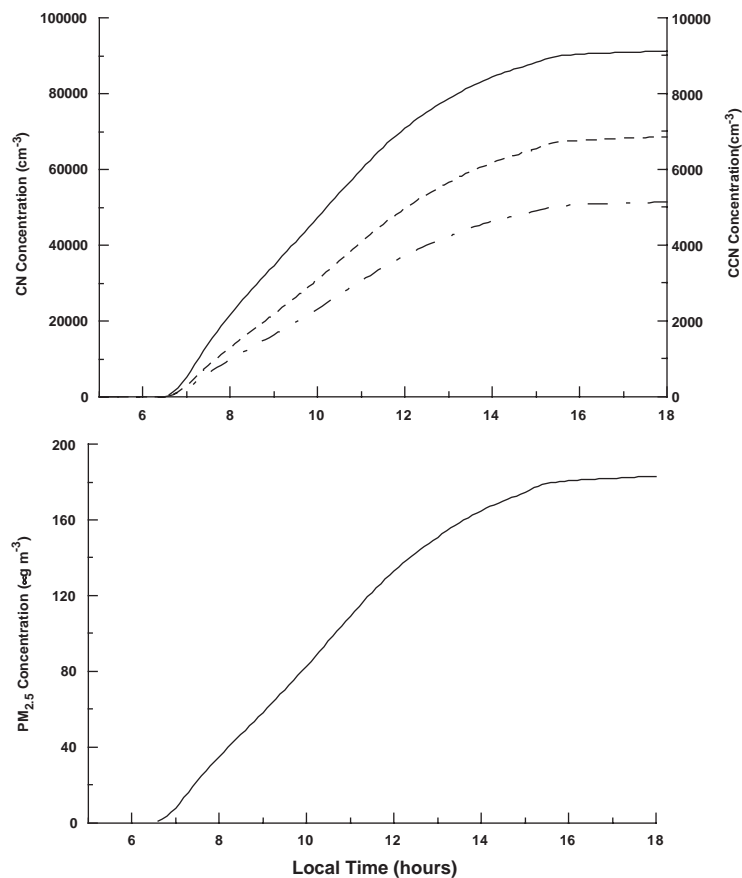


Fig. 6. The change in mass (bottom panel) and number concentration (top panel) as simulated with an aerosol box model are shown for particles greater than 0.03  $\mu\text{m}$  (light solid line), 0.06  $\mu\text{m}$  (light dashed line) and 0.1  $\mu\text{m}$  (dot-dashed line). The latter two lines simulate CCN concentrations for two organic compounds at 0.5% supersaturation.

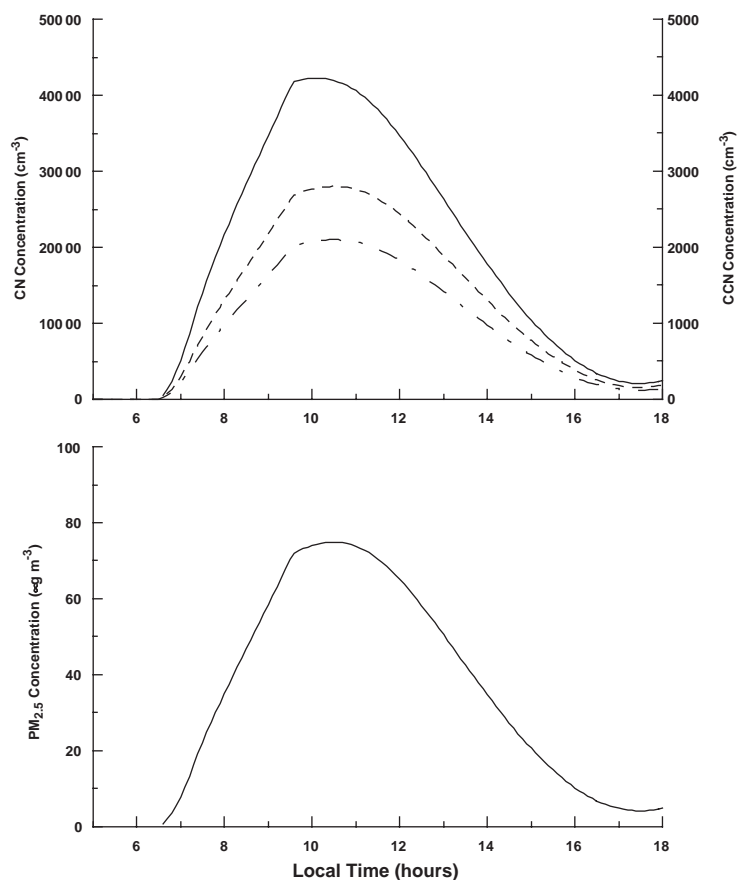


Fig. 7. The concentrations shown in Fig. 6 are shown after modification with a dilution factor that represents growth of the mixed layer.

where the effect is seen to offset the increase by constant emissions and growth by secondary processes.

The patterns that result from the model calculations are consistent with those that are observed. Many other physical and chemical processes control the formation and evolution of the particle spectra and the aerosol model is not expected to reproduce the exact features that are measured. The results are sufficient to support the hypothesis that photochemical processes will have a strong effect on trends in particle concentrations.

## 5. Summary

The trends in CN, CCN and PM<sub>2.5</sub> in Mexico City, observed during a 2 week measurement period, show similar patterns but the rate of increase in CCN concentrations is less than CN and PM<sub>2.5</sub>. This is linked to photochemical processes and instrument sensitivity. A size-resolved aerosol box model is used to simulate Mexico City conditions and the instruments used to measure the number and mass concentrations of CN,

CCN and PM<sub>2.5</sub>. The results of the model are consistent with observations that concentrations do not increase significantly until after sunrise, 30 min after the start of major emissions from traffic. The model also produces a difference between concentration increases measured by the CN and CCN that is consistent with the observations and that is sensitive to the critical diameter at a specific supersaturation. An additional dilution factor, derived from CO measurements explains the decrease in particle concentrations seen in the observations after midday. Finally, the maximum CN and CCN observations show no decrease over a 15 year period, indicating that pollution mitigation strategies by the government have had little impact on particles concentrations.

## Acknowledgements

The authors thank the University of Wyoming for their loan of the CCN counter used in this study, the personnel of RAMA for providing the gas and particle measurements from the Santa Ursula station and an

anonymous reviewer for many helpful suggestions and comments. This research was funded by CONACyT Grants # 32528 and 33319.

## References

- Allen, G., Sioutas, C., Koutrakis, P., Reiss, R., Lurmann, F.W., Roberts, P.T., 1997. Evaluation of the TEOM method for measurement of ambient particulate mass in urban areas. *Journal of Air Waste Management* 47, 682–689.
- Alofs, D.J., Liu, T.-H., 1981. Atmospheric measurements of CCN in the supersaturation range 0.013–0.681%. *Journal of Atmospheric Science* 38, 2772–2778.
- Carter, W.P.L., 1990. A detailed mechanism for the gas-phase atmospheric reactions of organic compounds. *Atmospheric Environment* 24A, 481–518.
- Changnon, S.A., Semonin, R.G., Auer, A.H., Braham, R.R., Hales, J.M., 1981. METROMEX: A Review and Summary. *Meteorological Monographs*, No. 118, American Meteorological Society Boston, MA., 181pp.
- Chuang, P.Y., Nenes, A., Smith, J.N., Flagan, R.C., Seinfeld, J.H., 2000. Design of a CCN instrument for airborne measurement. *Journal of Atmospheric and Oceanic Technology* 17 (8), 1005–1019.
- Chughtai, A.R., Miller, N.J., Smith, D.M., Pitts, J.R., 1999. Carbonaceous particle hydration III. *Journal of Atmospheric Chemistry* 34, 259–279.
- Corrigan, C.E., Novakov, T., 1999. Cloud condensation nucleus activity of organic compounds: a laboratory study. *Atmospheric Environment* 33, 2661–2668.
- Cruz, C.N., Pandis, S.N., 1997. A study of the ability of pure secondary organic aerosol to act as cloud condensation nuclei. *Atmospheric Environment* 31, 2205–2214.
- Delene, D.J., Deschler, T., 2000. Calibration of a photometric cloud condensation nucleus counter designed for deployment on a balloon package. *Journal of Atmospheric and Oceanic Technology* 17, 459–467.
- Delene, D.J., Deschler, T., Wechsler, P., Vali, G., 1998. A balloon-borne cloud condensation nuclei counter. *Journal of Geophysical Research* 103, 8927–8934.
- Durlak, S., Baumgardner, D., Raga, G.B., 1999. Examination of the evolution of Mexico City aerosols using an aerosol and photochemical box model. *Proceedings of the American Association for Aerosol Research Tacoma, USA*, 11–15 October.
- Fitzgerald, J.W., Spyers-Duran, P.A., 1973. Changes in cloud nucleus concentration and cloud droplet size distribution associated with pollution from St. Louis. *Journal of Applied Meteorology* 12, 511–515.
- Fitzgerald, J.W., Hoppel, W.A., Vietti, M.A., 1982. The size and scattering coefficient of urban aerosol particles at Washington, DC as a function of relative humidity. *Journal of Atmospheric Science* 39, 1838–1852.
- Harris, S.J., Maricq, M.M., 2001. Signature size distributions for diesel and gasoline engine exhaust particulate matter. *Aerosol Science* 32, 749–764.
- Harrison, R., Jones, M., Collins, G., 1999. Measurements of the physical properties of particles in the urban atmosphere. *Atmospheric Environment* 33 (2), 309–321.
- Herrera, J.R., Castro, J.J., 1988. Production of cloud condensation nuclei in Mexico City. *Journal of Applied Meteorology* 27, 1189–1192.
- Hindman, E.E., Hobbs, P.V., Radke, L.F., 1977. Cloud condensation nuclei from a paper mill, Part I: measured in clouds. *Journal of Applied Meteorology* 16, 745–752.
- Hitzenberger, R., Berner, A., Giebl, H., Kromp, R., Larson, S.M., Rouc, A., Koch, A., Marischka, S., Puxbaum, H., 1999. Contribution of carbonaceous material to cloud condensation nuclei concentrations in European background (Mt. Sonnblick) and urban (Vienna) aerosols. *Atmospheric Environment* 33, 2647–2659.
- Hori, M., Sachio, O., Murao, N., Yagamata, Y., 2003. Activation capability of water soluble organic substances as CCN. *Journal of Aerosol Science* 34, 419–448.
- Hudson, J.G., Frisbie, P.R., 1991. Surface cloud condensation nuclei and condensation nuclei measurements of Reno, Nevada. *Atmospheric Environment* 25A, 2285–2299.
- Jenkin, M.E., Clemmshaw, K.C., 2000. Ozone and other secondary photochemical pollutants: chemical processes governing their formation in the planetary boundary layer. *Atmospheric Environment* 34, 2499–2527.
- Kotzick, T.R., Niessner, R., 1999. The effects of aging processes on critical supersaturation ratios of ultrafine carbon aerosols. *Atmospheric Environment* 33, 2669–2677.
- Kotzick, R., Panne, U., Niessner, R., 1997. Changes in condensation properties of ultrafine carbon particles subjected to oxidation by ozone. *Journal of Aerosol Science* 28, 725–735.
- Montañez, R.A., García-García, F., 1993. Some urban and meteorological effects on the production of cloud condensation nuclei in Mexico City. *Atmósfera* 6, 39–49.
- Nenes, A., Chuang, P.Y., Flagan, R.C., Seinfeld, J.H., 2001. A theoretical analysis of cloud condensation nucleus (CCN) instruments. *Journal of Geophysical Research* 106, 3449–3474.
- Odum, J.R., Hoffmann, T., Bowman, F., Collins, D., Flagan, R., Seinfeld, J.H., 1996. Gas/particle partitioning and secondary organic aerosol yields. *Environmental Science and Technology* 30, 2580–2585.
- Odum, J.R., Jungkamp, T.P.W., Griffin, R.J., Flagan, R.C., Seinfeld, J.H., 1997. The atmospheric aerosol-forming potential of whole gasoline vapor. *Science* 276, 96–99.
- Quant, F.R., Caldow, R., Sem, G.J., Addison, T.J., 1992. Performance of condensation particle counters with three continuous-flow designs. *Journal of Aerosol Science* 23 (Suppl. 1), 405–408.
- Raga, G., Baumgardner, D., Kok, G., Rosas, I., 1999. Some aspects of boundary layer evolution in Mexico City. *Atmospheric Environment* 33, 5013–5021.
- Rosenfeld, D., 2000. Suppression of rain and snow by urban and industrial air pollution. *Science* 287, 1793–1796.
- Seinfeld, J.H., Pandis, S.N., 1996. *Atmospheric Chemistry and Physics*. Wiley, NY, 1323 pp.
- Smith, D.M., Chughtai, A.R., 1997. Photochemical effects in the heterogeneous reaction of soot with ozone at low concentrations. *Journal of Atmospheric Chemistry* 26, 77–91.
- Sun, Q., Wexler, A.S., 1998. Modeling urban and regional aerosols—condensation and evaporation near acid neutrality. *Atmospheric Environment* 32, 3527–3531.

- Vega, E., Mugica, V., Carmona, R., Valencia, E., 2000. Hydrocarbon source apportionment in Mexico City using the chemical mass balance receptor model. *Atmospheric Environment* 34, 4121–4129.
- Wexler, A.S., Lurmann, F.W., Seinfeld, J.H., 1994. Modeling urban and regional aerosols—I. Model development. *Atmospheric Environment* 28A, 531–546.
- Yu, S., 1999. Role of organic acids—formic, acetic, pyruvic and oxalic in the formation of cloud condensation nuclei (CCN): a review. *Atmospheric Environment* 33, 2647–2659.
- Zhang, K.M., Wexler, A.S., 2002. Modeling the number distributions of urban and regional aerosols: theoretical foundations. *Atmospheric Environment* 36, 1863–1874.